Voltage Diffusion in an Insulating Sheet with a Conductive Layer

John Szafraniec[1], Robert Brearey[1], and Kelly Robinson[2]
[1]Carestream Health, Inc., Oakdale Media Laboratory, Oakdale, MN
phone: (1) 651-393-1461
e-mail: john.szafraniec@carestreamhealth.com

[2]Electrostatic Answers, LLC, Rochester, NY

***Abstract*—Electrostatic charge causes transport problems with sheet media that are designed for use in inkjet and laser printers. Charge causes sheets to misfeed from a stack, as they are fed into the printer, or cause sheets to jam as they are conveyed through the equipment. By providing a conductive layer within the sheet itself, the current flowing through the conducting layer affects the electrostatic performance of the media. The conductive layer may be the paper core of resin-coated paper, or it may be a layer within the sheet itself that is specifically formulated for conductivity. While this current flow may improve the reliability of media transport, it can also aggravate sheet sticking.**

We report experimental measurements of the surface voltage of a sheet of media with a buried conducting layer. The sheet is lying flat on a grounded plate. Voltage is applied to an electrode that is clamped to one end of the surface of the sheet. The surface potential over the length of the sheet varies as current flows through the conductive layer. The time constant governing the transient current ranges from 10–1000 seconds for conductive layers with sheet resistivities in the range of 10^{+9} to 10^{+11} Ω/□.

We present the results of three models that predict the charge flow in the system. First, a lumped-parameter electromechanical model predicts the electrostatic sticking force, assuming that the conducting layer is an equipotential. A first-principles model is based on an equivalent circuit including the layer resistivity, and a finite-element model includes the effects of fringing electric fields. The key results are that charge flows in the conducting layer that increases the electrostatic force, surface voltage is governed by the diffusion equation, and the sheet resistivity and capacitive coupling to the grounded plate determine the diffusion constant. Model predictions are confirmed by our experimental results.

I. Introduction

Electrostatic charge causes stacked sheets of media to stick to each other, resulting in misfeeds from the top of the stack. Figure 1 depicts a simple printer, scanner, or other device that feeds a sheet of media from an input stack, transports the sheet through the device, and collects the finished sheet in an output bin. Excessive static charge on the top sheet of the input stack causes the sheet to stick to the input stack, which reduces the reliability of sheet feeds. As the sheet is transported through the device, charge also causes the sheet to stick to rollers, guides, and other objects in the transport path, which results in jams that reduce the reliability of sheet transport.

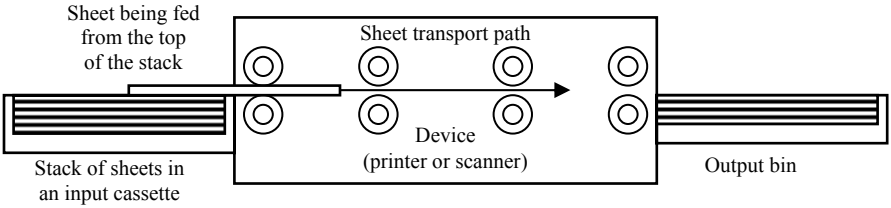

Fig. 1. A printer or scanner feeding sheets of media from the top of an input stack, transports the sheets through the device, and collects the finished sheets in an output bin.

Preventing electrostatic problems during the transport of flexible media has been extensively studied. Improving static performance by providing a conductive layer on the surface of flexible media dates back to at least 1938 [1]. There are several disadvantages to using a conductive layer on the surface of films or sheets. The layer is exposed to the ambient environment and its properties may change with the relative humidity. Also, the chemicals in the conductive layer may change over time, limiting product shelf life. And, if the media must undergo chemical processing, such as photographic development, the surface layer may cause undesirable foaming and be washed away, compromising future static performance.

Burying the conductive layer within the media eliminates many problems and effectively suppresses static discharges and dust attraction. Burying a layer specifically formulated for conductivity beneath a protective overcoat dates back to at least 1980 [2]. In the same way, resin-coated paper for photographic printing has benefited from the conductivity of the paper core.

However, buried layers aggravate sheet-sticking problems. Buried layers are electrically isolated, so charge within the layer cannot flow easily to ground. As the sheet is fed from the input stack and transported through the device, charge flows through the conductive layer.

Understanding this flow of charge within the buried conductive layer is fundamental to predicting static performance. Because it is difficult to directly measure the current flowing in the buried conductive layer, we measured the surface voltage of a sheet that was lying flat on a grounded plate. Voltage was applied to an electrode that was clamped to one end of the surface of the sheet to electrically excite the system. The surface potential over the length of the sheet varied as current flowed through the conductive layer.

We measured the time constant governing the transient current to be in the range from 10–1000 seconds for conductive layers with sheet resistivities in the range of 10^{+9} to 10^{+11} Ω/□. The time constant governing the transient current is comparable to the mechanical time, which characterizes feeding and sheet transport. Therefore, there is a strong coupling between sheet motion and electrical forces [3].

We report the results of three models that predict the charge flow in a conductive layer that is buried within a sheet. A lumped-parameter electromechanical model predicts electrostatic sticking caused by charge that flows during sheet feeding, which accumulates in the area of the sheet that is in contact with the stack. A first-principles model is based on an equivalent circuit that includes the resistivity of the layers, and a finite-element model includes the effects of fringing electric fields. The key result is that surface voltage is

governed by the diffusion equation, and the sheet resistivity and capacitive coupling to the grounded plate determine the diffusion constant.

II. THEORY

A. Lumped-Parameter Electromechanical Model

Figure 2 illustrates a lumped-parameter electromechanical model [4] for feeding a sheet from the top of a stack. The sheet is represented by an insulating slab with a dielectric constant κ_r. The buried conducting layer is distance d above the lower surface and is distance h below the upper surface. A "virtual air gap" of height δ exists between the sheet and the top of the stack. The electric field across this air gap causes the sticking force.

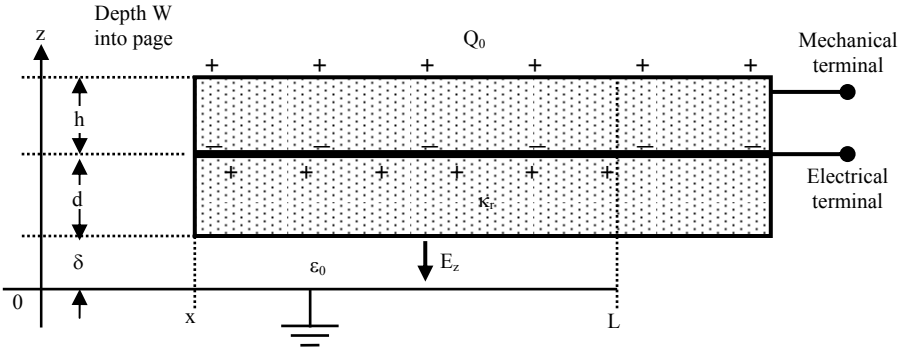

Fig. 2. Simplified model for feeding the top sheet from a stack represented by a grounded plate.

An initial charge Q_0 on the upper surface of the sheet is represented by six positive charges. The conducting layer has an image charge $-Q_0$ represented by six minus charges. Because the conducting layer is electrically isolated, charge is conserved by adding six positive charges that are mobile and will move as the sheet is fed to maintain the conducting layer at a uniform potential.

The voltage of the conductive layer as a function of initial charge and position x is given in (1).

$$V_0 = \frac{Q_0}{C_{eff}} = \left[\frac{\frac{d}{\kappa_r} + \delta}{\varepsilon_0 (L - x) W} \right] Q_0 \qquad (1)$$

The voltage of the conductive layer increases as the sheet is pulled from the top of the stack, and charge concentrates where the top sheet remains in contact with the stack. The electric field across the virtual air gap is given in (2).

$$E_z = \frac{\sigma_0}{\varepsilon_0} = \frac{Q_0}{\varepsilon_0 (L - x) W} \qquad (2)$$

The electric field is independent of the air gap height δ and increases as the sheet is pulled from the top of the stack. The energy stored in the electric field is given in (3).

$$W_e = \frac{Q_0^2}{2C_{eff}} = \frac{Q_0^2}{2}\left[\frac{\frac{d}{\kappa_r}+\delta}{\varepsilon_0 (L-x) W}\right] \tag{3}$$

The electric force is the change in energy with position, as in (4).

$$f_e = -\frac{\partial W_e}{\partial x} = -\frac{Q_0^2\left(\frac{d}{\kappa_r}+\delta\right)}{2\varepsilon_0 W (L-x)^2} \tag{4}$$

TABLE 1: GEOMETRIC, PHYSICAL CONSTANTS, AND INITIAL VOLTAGE

Parameter	Value	Units	Description
d	200	μm	thickness of a sheet
δ	4	μm	thickness of air gap between sheet and grounded plate
ε_0	8.854	pF/m	permittivity of free space, physical constant
h	4	μm	thickness of the insulating layer above the conducting layer
κ_r	2.5		relative dielectric constant of support
L	0.432	m	17 inch length of a sheet
V_0	100	V	applied voltage, initial condition
W	0.356	m	14 inch width of a sheet
Values computed from initial conditions			
f_e		N	electric force in (3)
σ_0	10.5	μC/m^2	initial charge density
Q_0	1.62	μC	computed using V_0 using (7)

Table 1 shows dimensions and initial conditions, which are typical for our experiment, using a 14×17 inch sheet on a grounded plate. Figure 3 shows a contour plot of the electric force as a function of the initial voltage on the sheet and contact distance with the top of the stack.

This lumped-parameter electromechanical model reveals the following results:

1. The electric force opposes feeding.
2. The electric force increases strongly with the square of the initial charge on the sheet.
3. The electric force increases sharply as charge in the conductive layer concentrates into a small area.
4. Given that double feeds occur when the electric force is on the order of the weight of a single sheet (0.1 to 1.0 N), jamming should occur when the initial voltage exceeds about 20 V. Below this level, the sticking force exceeds 0.1 N only when (L–x) is very small. When (L–x) is on the order of the sheet thickness, equations (2), (3), and (4) are no longer valid because the electric field is no longer uniform.

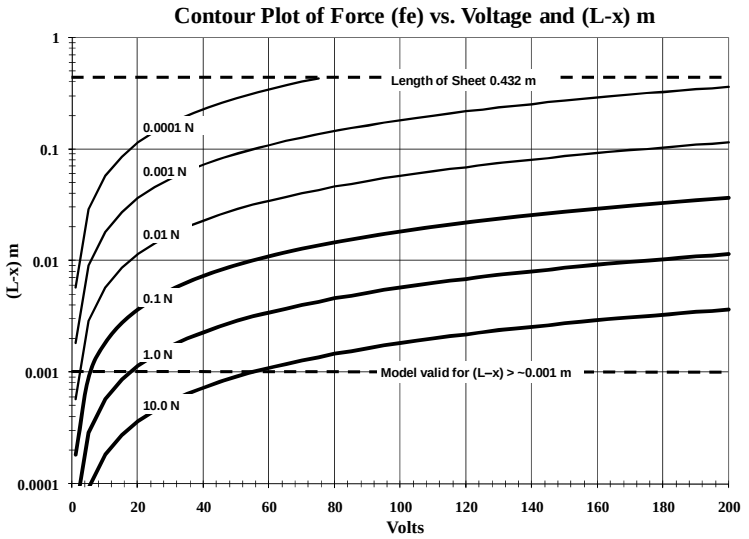

Fig. 3. Contour plot of the electric force as a function of the initial voltage and contact distance.

Note that in this lumped-parameter electromechanical model, the buried layer is highly conducting so that charge moves instantaneously as the sheet moves. An equivalent circuit model follows, which includes the effect of the resistivity of the buried layer.

B. Equivalent Circuit Model

Figure 4 illustrates the equivalent circuit for a sheet on a grounded plate.

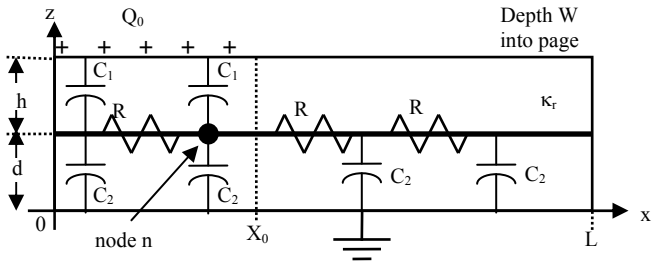

Fig. 4. Equivalent circuit model for a sheet on a stack. The top of the stack is represented by a grounded plate. The conductive layer is electrically isolated and uncharged. The resistance of the conductive layers is included, as well as the capacitive coupling between the surface charge and the conductive layer.

The sheet resistivity of the conductive layer is included as a series of resistors R given in (5).

$$R = \rho_S \frac{\Delta x}{W} \tag{5}$$

With this model, we analyze an initial charge distribution that is a band along the leading edge of the sheet. This band of surface charge is coupled to the conductive layer by capacitances C_1 given in (6).

$$C_1 = \varepsilon_0 \kappa_r \frac{W \Delta x}{h} \tag{6}$$

The conductive layer is coupled to the grounded plate through capacitance C_2 given in (7).

$$C_2 = \varepsilon_0 \kappa_r \frac{W \Delta x}{d} \tag{7}$$

Applying the Kirchhoff Current Law (summing the currents) into node n results in (8).

$$\frac{V_{n-1} - V_n}{R} + C_1 \frac{d(V_S - V_n)}{dt} = \frac{V_n - V_{n+1}}{R} + C_2 \frac{dV_n}{dt} \tag{8}$$

Substituting (5) through (7) into (8) and taking the limit as Δx approaches 0 gives (9).

$$\rho_S \varepsilon_0 \kappa_r \left(\frac{1}{d}\right) \frac{\partial V}{\partial t} - \frac{\partial^2 V}{\partial x^2} = 0 \tag{9}$$

The governing equation (9) is revealing in two ways:

1. The voltage is governed by the diffusion equation.
2. The diffusion time is determined by the resistivity of the conductive layer and by the capacitive coupling of the conductive layer to the grounded plate (remaining stack).

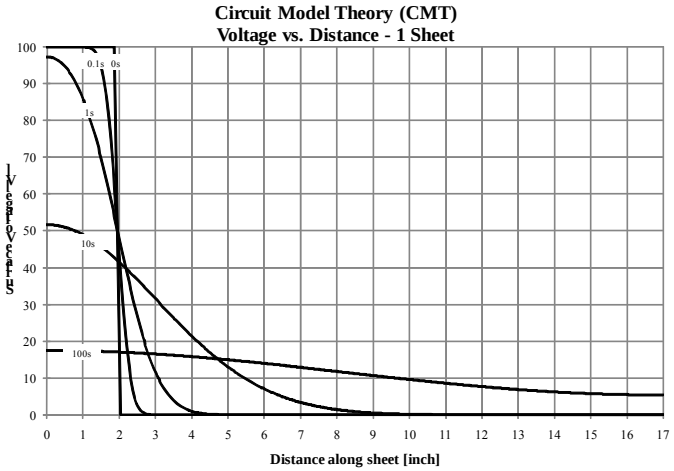

Fig. 5. Voltage plotted as a function of distance along the sheet surface with a 100 V initial surface voltage along a 2-inch band at the edge of the 17-inch sheet. As time progresses, the voltage approaches a uniform voltage distribution of 11.6 V.

Figure 5 shows a solution of the diffusion equation (9) solved numerically using the Crank-Nicholson differencing scheme [5]. Differencing converts the continuous partial

differential equation into a system of algebraic equations that is solved by LU decomposition of a band diagonal matrix with iterative improvement [6]. The solution shown uses the geometric values in Table 1 for an initial voltage of 100 V on a 2-inch band along one edge of a 17-inch sheet having a conductive layer with a sheet resistivity of $3\times10^{+10}$ Ω/□. The solution domain has been differenced into 1000 segments.

The key result is that the voltage transient persists for much longer than the typical feeding sequence for printers. Charge will flow within the conductive layers in response to the mechanical movement of the media.

The implicit assumption in this equivalent circuit model is that the electric fields are z-directed. Specifically, the electric fields have no x component. Analysis using the finite element method (FEM) to solve for the voltage includes both x- and z-directed electric fields.

C. ANSYS FEM Model

1) Electromagnetic theory

FEM is a powerful and flexible technique for numerically solving partial differential equations. Commercially available FEM programs are capable of solving the general form of the governing (Maxwell's) equations given in (10).

$$\nabla\cdot\vec{D}=\rho_{vol} \qquad \nabla\cdot\vec{B}=0$$
$$\nabla\times\vec{E}=\frac{\partial\vec{B}}{\partial t} \qquad \nabla\times\vec{H}=\vec{J}+\frac{\partial\vec{D}}{\partial t} \tag{10}$$

TABLE 2: ELECTROMAGNETIC QUANTITIES AND PARAMETERS

Parameter	Units	Description
B	Webers/m^2	magnetic flux density
D	Coulombs/m^2	electric flux density
ε_0	Farads/m	permittivity of free space
E	V/m	electric field
H	A/m	magnetic field
J	A/m^2	electric current density
κ_r	dimensionless	relative dielectric constant
μ	Henry/m	magnetic permeability
ρ_{vol}	Coulomb/m^3	volumetric charge density
σ	Seimens/m=1/(Ohm-m)	electrical conductivity
t	s	time
V	V	electric potential

The electromagnetic parameters and quantities are summarized in Table 2. The constitutive relations are given in (11).

$$\vec{D}=\varepsilon_0\,\kappa_r\,\vec{E};\quad \vec{B}=\mu\,\vec{H};\quad \vec{J}=\sigma\,\vec{E};\quad \nabla\cdot\left(\vec{J}+\frac{\partial\vec{D}}{\partial t}\right)=0 \tag{11}$$

For electrostatic phenomena, terms involving magnetic quantities are negligible and the governing equations simplify to (12).

$$\nabla \times \vec{E} = 0 \quad \Rightarrow \quad \vec{E} = -\nabla V$$
$$\nabla \cdot (\sigma \nabla V) + \nabla \cdot \left(\varepsilon_0 \kappa_r \nabla \frac{\partial V}{\partial t} \right) = 0 \tag{12}$$

With these constitutive relations and simplifying assumptions, conduction and dielectric effects are taken into account.

2) Solution with a commercially available finite element code (ANSYS)

A two-dimensional, cross-sectional finite element model was used to evaluate the time-dependent charge flow in a 14×17-inch sheet. This model assumed that the flow across the width of the sheet was negligible and the flow down the page was dependent on resistivity and capacitive coupling to the ground plate. Initially, we took sheet dimensions to be 432 mm long by 195 μm thick. The thickness of the back coat and Celnax conductive layers totaled 3 μm. However, this model would not run because the element aspect ratio was too large (>1000:1) to meet the ANSYS model check requirements. Refining the mesh allowed the system to run, but it took several hours per iteration. This resulted in an unacceptable time constraint for the number of planned iterations.

An alternative approach was to shorten the length of the sheet while maintaining the actual thicknesses, as illustrated in Figure 6. The sheet resistivity is determined by requiring the time constant for voltage diffusion to be identical to that for the full-sized sheet. This resulted in an acceptable solution time (<5 min. per run) with seemingly good results.

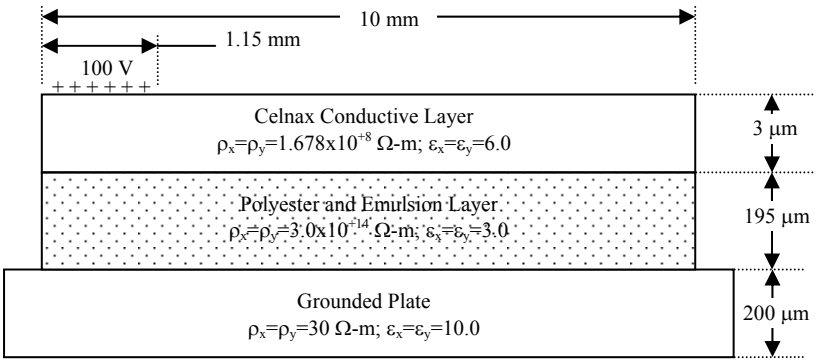

Fig. 6. Shown are the geometric and material properties used for the ANSYS finite element model.

Sheet resistivity is related to volume resistivity as in (13).

$$\rho_{\text{Sheet}}\left[\frac{\Omega}{\square}\right] = \frac{\rho_{\text{Volume}}[\Omega - \text{m}]}{d_{\text{Layer}}[\text{m}]} \tag{13}$$

The time constant τ for charge relaxation on a sheet resting on a grounded plate [3] is given in (14).

$$\tau = \frac{\left(\frac{\rho_{Volume}}{d_{Layer}}\right)\varepsilon_0 L^2}{\pi^2\left(\frac{d_{Poly}}{\kappa_{Poly}} + \frac{d_{Emulsion}}{\kappa_{Emulsion}}\right)} \qquad (14)$$

Scaling the sheet length L in our model calculation, we needed to adjust the resistivity ρ_{ANSYS} so that the time constant τ matched the full sized sheet as in (15).

$$\rho_{ANSYS}\left[\frac{\Omega}{\square}\right] = \left(\frac{L_{Sheet}}{L_{ANSYS}}\right)^2 \rho_{Sheet}\left[\frac{\Omega}{\square}\right] \qquad (15)$$

Figure 7 shows the equipotential contours in the immediate vicinity of the charge strip for the geometry shown in Figure 6, where parameters are selected to match the solution for the full sheet using the circuit model shown in Figure 3.

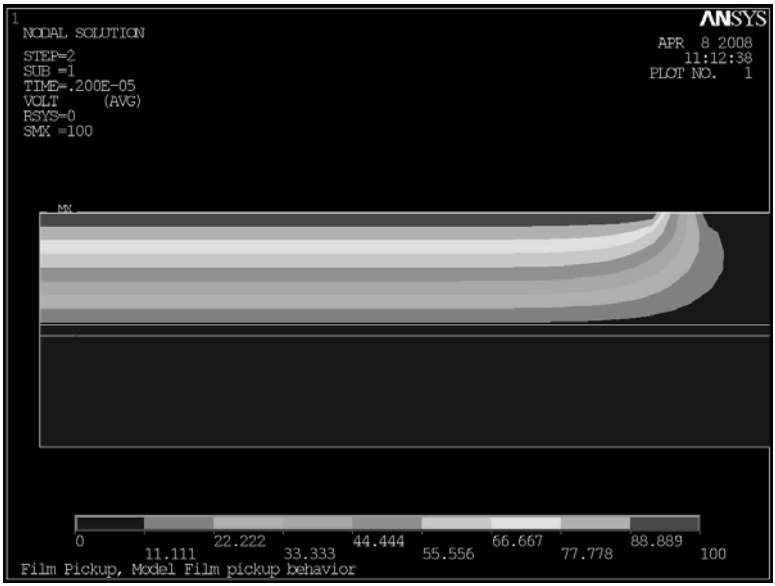

Fig. 7. Equipotential computed by ANSYS in the immediate vicinity of the 100 V strip of charge along the edge of the film.

Note that the electric field has a significant horizontal component where the contours are vertical. Figure 8 is a plot of the voltage on the surface of the sheet as a function of distance along the sheet.

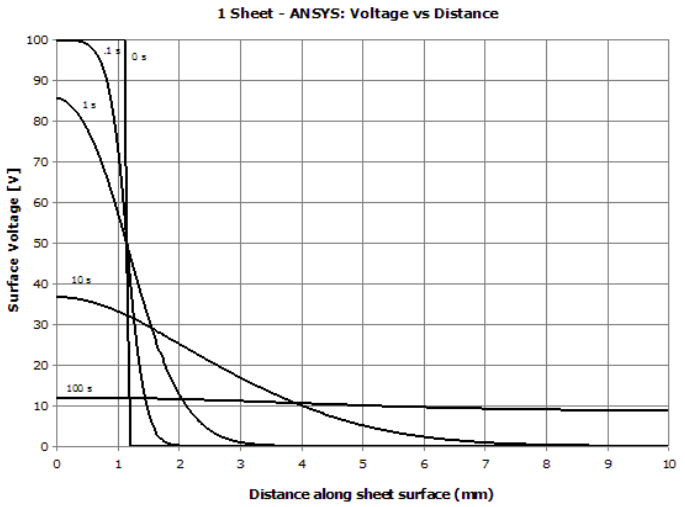

Fig. 8. Surface potential as a function of distance computed by ANSYS for the idealized case of a band of charge resulting in a uniform potential of 100 V along the leading edge of a sheet.

Figure 9 is a plot of the residual voltage, which is the difference between voltage V_{ANSYS} computed using ANSYS and voltage V_{CMT} computed using the circuit model. The surface potential, as a function of distance and time computed using ANSYS and CMT, are very similar. From the numerical data, the total, initial surface charges for ANSYS and CMT are the same to within 1.5%. Through the time integration, both ANSYS and CMT conserve charge to within 1.0%.

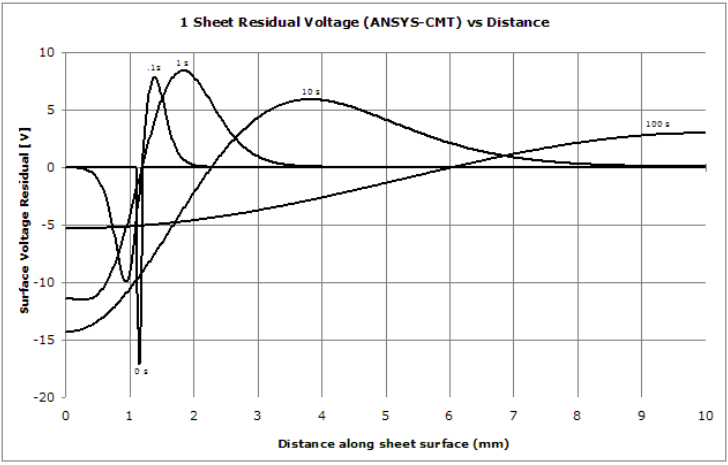

Fig. 9. Residual voltage V_{ANSYS}-V_{CMT} as a function of distance for several different time points.

III. Experimental Methods and Materials

An experiment was performed to verify the analytical model predictions at three different sheet resistivities at two different probe locations.

A. Experimental Method

A set of 1.4 inch (35 mm) × 17 inch (432 mm) strips of *Kodak DryView* laser imaging film consisting of a 175 μm thick polyester base, with a 20 μm emulsion layer (non-conducting) on the front side of the strips and a Celnax conductive layer on the back sides was used for the experiment. The Celnax layer had a non-conducting polymeric overcoat of 2 μm. The overcoat also covered a roughening agent, which resulted in a gap from the Celnax layer to the back surface that ranged from 2 to 7 μm. As illustrated in Figure 10, the film was placed emulsion side down on a grounded plate, resulting in a 195 μm dielectric layer between the conductive layer and the grounded plate. Three samples each, of three different sheet resistivities, 9.5, 10.6, and 11.2 log Ω/□ were tested. The experiments consisted of applying a constant 100 V potential to a 1 inch (25.4 mm) long area across the full width of the strip and measuring the potential at 14 inches (178 mm) and 17 inches (356 mm) from the leading edge of the film.

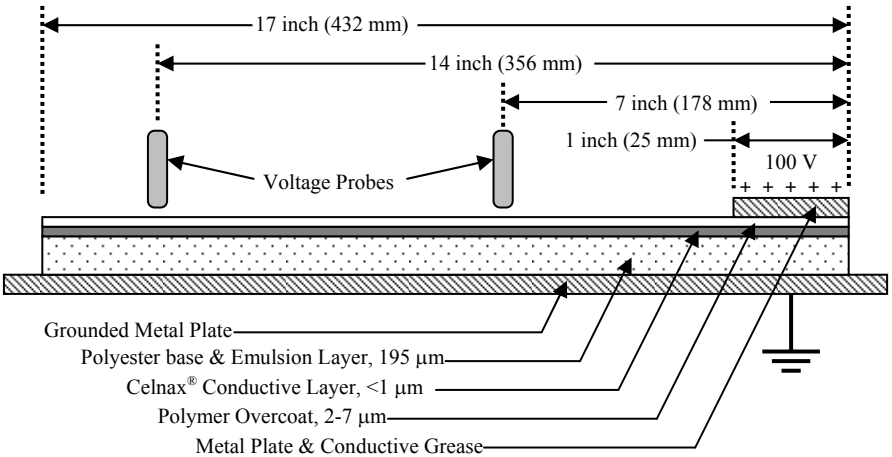

Fig. 10. Experimental setup for measuring charge flow.

Two approaches for applying a known charge were unsuccessful before the current method was developed. The first method used a grid-controlled ionizer on a full-sized (14 × 17 inch) sheet of film. The inherent Gaussian distribution of the charge could not generate the desired square profile distribution of the potential. Although it would be possible to change the boundary conditions in the model to match the Gaussian profile, a bigger problem with the method was the inability to explicitly control the magnitude of the potential. This resulted in an ill-defined boundary condition and resulted in poor correlation to the analytical models.

A second approach was to use a high-voltage power supply and a conducting metal strip clamped against the lead edge of the 14 × 17 inch sheet of film with conductive

grease between the metal and film. This approach worked better than the first approach, but it was highly sensitive to the contact pressure variation of the metal along the leading edge of the film. This resulted in very poor repeatability of the measurements on the same sheet of film.

The method used in the third approach, shown in the photograph in Figure 11, was the same as the second approach, except the film sample was a 1.4-inch (35 mm) wide × 17-inch long strip. This allowed the contact between the film and the grounded plate to be adequately uniform, and it provided reasonably good results.

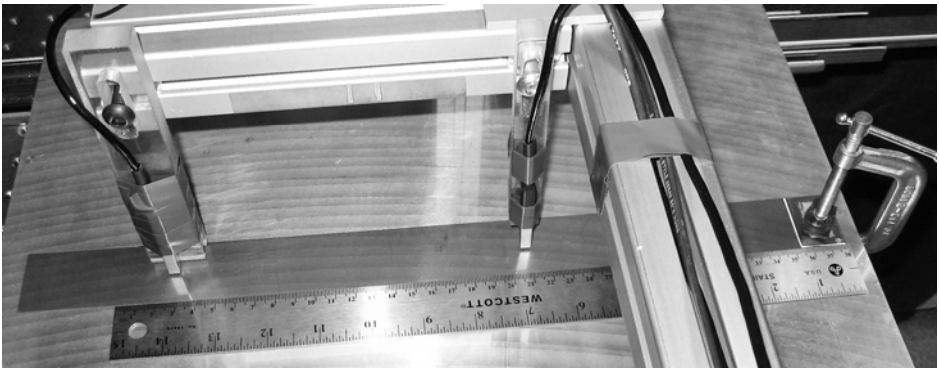

Fig. 11. Test strip of film on a grounded plate with the two voltage probes and the charging plate (right side) clamped to the film

Equipment used to apply the known potential and measure the downstream response was:

- High-voltage power supply – Fluke 415B
- Two non-contact voltage probes – Trek model 400
- Data acquisition system – DATAQ DI-158U, set at 2.5 samples per second

B. Experimental Results

Figures 12 and 13 show the raw experimental data for the three samples, with the three different sheet resistivities, at the 7- and 14-inch positions. The raw data has considerable spread among the three replicates but does show reasonable correlation for a given sample at the two different measurement positions.

An attempt to fit a first-order RC circuit model to the data showed there was a significant nonlinearity deviation for all of the resistivity levels. Given that the intent of the experiment was to verify that analytical models were giving realistic behavior, a point-by-point average of the three replicates, as shown in Figure 14, was considered to be the best method of comparing the experimental results to the analytical model. Table 3 shows the error estimate for the fit as a root mean square error (RMSE).

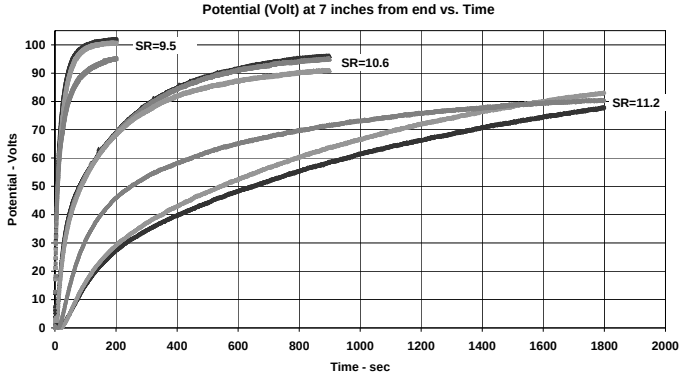

Fig. 12. Potential at 7 inches (178 mm) from the edge for three samples at sheet resistivities of 9.5, 10.6, and 11.2 log Ω/□. The data shows significant variability for a given sheet resistivity. As expected, the higher sheet resistivity exhibits a longer time constant.

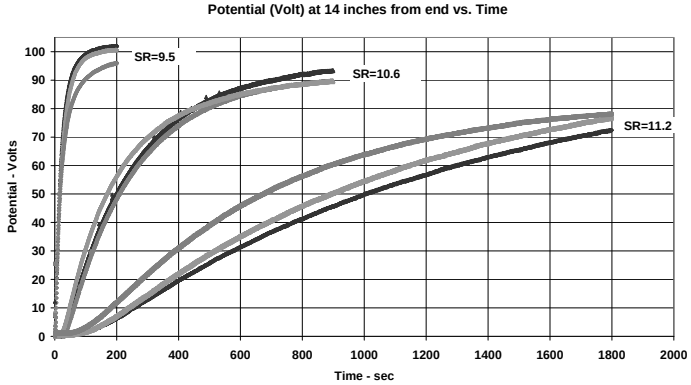

Fig. 13. Potential at 14 inches (356 mm) from the edge for three samples at sheet resistivities of 9.5, 10.6, and 11.2 log Ω/□. The data shows the same behavior as the 7-inch position (Fig. 11) but with a slight increase in the time constant.

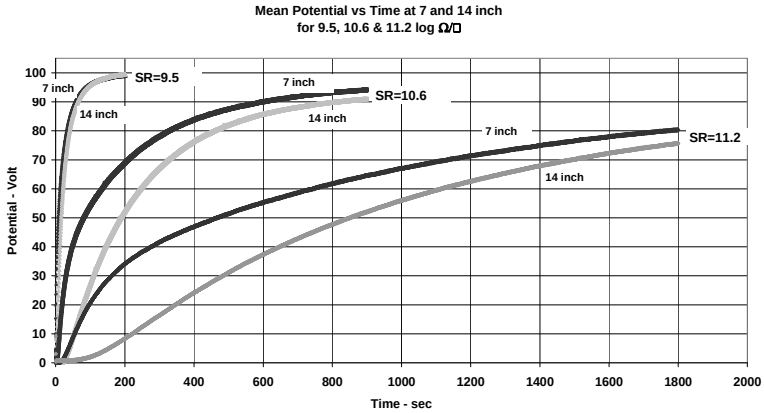

Fig. 14. The plot shows the mean of the three samples for each sheet resistivity and probe position. Note the significant delay before the potential begins to change for the higher resistivity and longer probe distance.

TABLE 3: VARIABILITY ESTIMATE FOR THE TEST DATA

Resistivity (log Ω/□)	Distance (inch)	RMSE (Volt)
9.5	7	4.6
9.5	14	4.1
10.6	7	1.6
10.6	14	2.1
11.2	7	6.9
11.2	14	5.8
		Pooled RMSE = 4.6

The RMSE may be thought of as the standard deviation after the mean has been subtracted from the raw data. The pooled RMSE (4.6 V) is the root sum square (RSS) of the individual RMSEs and is the best estimate of the overall variability in the data. Assuming a normally distributed system, this would imply the experimental method would result in 95% of the data to fall with ±9.2 V, out of 100 V peak, of the mean predicted line.

From previous work, a number of contributors have been identified as causing the variability. The average sheet resistivity is quite uniform within a sheet, but the point-to-point variation is unknown. We know there is significant variation on the conductive/capacitive path from the metal plate, used to charge the system, through the overcoat to the Celnax conductive layer in the sheet.

There also can be variability in the capacitive coupling to the grounded plate due to small air gaps between the sheet and plate. Although there is room for improvement in the experimental method, the results are sufficiently well behaved to allow a correlation to the analytical methods.

C. Experimental/Analytical Correlation

Figures 15, 16, and 17 show the correlation between the ANSYS model and the mean of the test data for each sheet resistivity. In general, the ANSYS-predicted voltage is within two standard deviations of the test mean. When the time to reach a particular voltage was used as a metric, all of the test data was within 35% (worst case was a sheet resistivity 9.5 at 14 inches) of the ANSYS predictions.

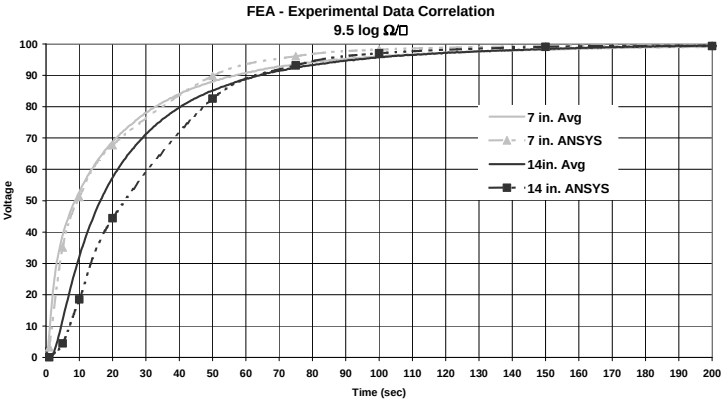

Fig. 15. Comparison of the ANSYS predictions with the mean of the test data for the sheet resistivity of 9.5 log Ω/ □. The worst-case time deviation (<35%) occurs near 30 seconds for the 14-inch probe distance.

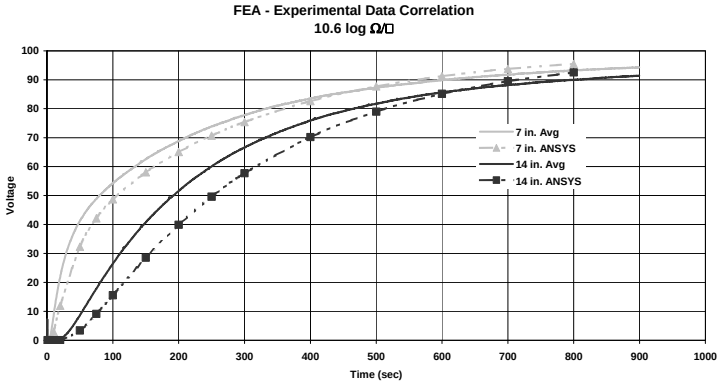

Fig. 16. Comparison of the ANSYS predictions with the mean of the test data for the sheet resistivity of 10.6 log Ω/ □. The worst-case time deviation (25%) occurs near 300 seconds for the 14-inch probe distance.

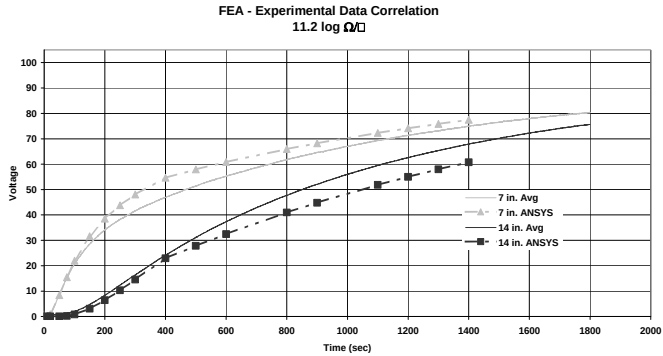

Fig. 17. Comparison of the ANSYS predictions with the mean of the test data for the sheet resistivity of 11.2 log Ω/ □. The worst-case time deviation (<35%) occurs near 400 seconds for the 7-inch probe distance. The 7-inch data is the only one that shows the ANSYS prediction occurring faster than the mean test data through the steepest part of the curve.

Although the correlation is less than perfect between the ANSYS model and test data, the amount of deviation is reasonably good when the inherent difficulty in getting repeatable test data is taken into account. The ANSYS model exhibits the same basic behavior over the entire investigated time range and will be useful for performing sensitivity studies on the system.

IV. Discussion

One of the problems in testing a highly variable system is that it requires many replicates to gain adequate resolution to make good design decisions. This can be very costly and time consuming. The intent of this work was to look at two analytical modeling methods that could provide adequate guidance in a more cost-effective manner.

The circuit model and ANSYS model correlate extremely well with each other. This implies the fringing field effect is a relatively small driver in the system. One important limitation of both predictive models would be if the fringing fields became sufficiently large to create a static discharge. Although not included in the model, the predictions from the models can be compared to the Paschen limit to see if the models are approaching this limitation.

To quote the statistician George Box, "All models are wrong, some are useful." Both modeling approaches correlate sufficiently to the test data to provide useful information about the global behavior of a system. This is extremely helpful in understanding the behavior of a system that is very difficult to quantify in a repeatable manner with test-only approach.

References

[1] A. D. Slack et al., "Antistatic Photographic Film," U.S. Patent 2 118 059, May 24, 1938.
[2] C. Guestaux, "Radiation-sensitive elements having an antistatic layer containing amorphous vanadium pentoxide," U.S. Patent 4 203 769, May 20, 1980.
[3] K. Robinson, "Charge Relaxation Due to Surface Conduction on an Insulating Sheet Near a Grounded Conducting Plane," *IEEE Trans. Indust. Appl.*, vol. 40, No. 5, pg. 1231–1238, 2004.

[4] H. H. Woodson and J.R. Melcher, *Electromechanical Dynamics (Part I)*, New York, NY: Wiley, 1968, Chapter 3, pp. 60–88.
[5] W. H. Press et al., *Numerical Recipes in C (Second Edition)*, Cambridge: Cambridge University Press, 1992, Chapter 19, pp. 847–851.
[6] Ibid., Chapter 2, pp. 50–58.